The elasto-plastic behaviour of three-dimensional stochastic fibre networks with cross-linkers

Y.H. Ma [a], H.X. Zhu [a,*], B. Su [b], G.K. Hu [c], R. Perks [a]

[a] School of Engineering, Cardiff University, Cardiff CF243AA, UK
[b] School of Oral and Dental Sciences, University of Bristol, Bristol BS12LY, UK
[c] School of Aerospace Engineering, Beijing Institute of Technology, Beijing 100081, China

A B S T R A C T

Fibre network materials constitute a class of highly porous materials with low density, promising for functional and structural applications; however, very limited research has been conducted, especially on simulation and analytical models. In this paper, a continuum mechanics-based three-dimensional periodic beam-network model has been constructed to describe the stochastic fibre network materials. In this model, the density of the cross-linkers is directly related to the relative density of the fibre network materials, and the cross-linkers are represented by equivalent beam elements. The objective of this work was to delineate the elasto-plastic behaviour of the stochastic fibre network materials. Characteristic stress and strain derived from the total strain energy density have been adopted to reveal the yielding behaviour of the fibre networks. The results indicate that the stochastic fibre network materials are transversely isotropic. The in-plane stiffness and strength are much larger than those in the out-of-plane direction. For the fibre network materials with a small relative density, the relationship between the uniaxial yield strength and the relative density is a quadratic function in the x direction and is a cubic function in the z direction, which agree well with our dimensional analysis and are consistent with the relevant experimental results in literature. The yield surface depends strongly on the relative density and the connection between fibres.

1. Introduction

Cellular materials have been of great interest to engineers and scientists due to their attractive mechanical and physical properties and their wide applications. Foams and honeycombs, which are categorized as cellular materials, have been extensively studied (Banhart, 2001; Chen et al., 1999; Gibson and Ashby, 1997; Silva and Gibson, 1997; Zhu et al., 2000, 1997). As Gibson and Ashby (1997) described, the four major engineering applications of cellular materials are thermal insulation, packaging, structural use and buoyancy attributed to their low thermal conductivity, high compressive strength, high stiffness and low density. With the same attractive properties as other cellular materials, porous fibrous materials are less researched and understood because of their more complex geometry. Some techniques have been developed to pro-

duce fibrous materials, for instance, fibre pull-out techniques (Xi et al., 2011) for porous metal fibre sintered sheets (MFSSs) (Jin et al., 2013) which can be used in sandwich panel cores, and electrospinning techniques (Huang et al., 2003; Zhang et al., 2008) for polymer fibre scaffold used in drug delivery and tissue engineering (Sill and von Recum, 2008). In the architecture of honeycombs and foams, cells are distinct and a single idealized unit cell can be used to represent the microstructural features, e.g., 2D honeycombs in which a representative element can be a single triangular, square or hexagonal cell (Gibson and Ashby, 1997; Zhu et al., 2012). Many analytic and simulation models have been developed to investigate the macro-mechanical behaviour of honeycombs and foams (Chen et al., 1999; Redenbach, 2009; Silva and Gibson, 1997; Youssef et al., 2005; Zhu et al., 2001, 2000, 1997). In contrast, the architecture is much more complicated for fibrous materials, for instance, felt, as it is very difficult to define an individual cell in the architecture. Paper is a typical stochastic fibrous material which is, to some extent, the most familiar one to most of us. Porous metal fibre sintered sheets (MFSSs) are metal fibrous materials with good balance between density and strength, and have a great potential for functional and structural applications. MFSSs are produced by overlapping the randomly distributed fibres by air-laid web-forming technology before compressing and sintering into three-dimensional materials with a fibre network (Xi et al., 2011). Experiments (Zhao et al., 2013) show that the MFSSs are transversely isotropic and that the in-plane stiffness and strength are much higher than those in the out-of-plane direction, which is different from foams or honeycombs. Connectivity in the fibre network materials plays a significant role in determining the mechanical properties. It was found that the in-plane deformation of porous materials with high nodal connectivity is stretching dominated. In contrast, the deformation mode of low density two-dimensional hexagonal honeycomb is a combination of cell wall stretching and bending when the nodal connectivity is low (Symons and Fleck, 2008). Jin et al. (2013) developed a two-dimensional random micromechanics beam model to investigate the in-plane elasto-plastic behaviour of MFSSs (Jin et al., 2013). In their model, all the fibres are completely overlapped with each other to form a two-dimensional stochastic fibre network, which leads to very strong bonding connections and high nodal connectivity between fibres. Xi et al. (2011) proposed that the mechanical properties of metal fibre porous materials are highly dependent upon the fibre-fibre joints and the number of metallurgy nodes. The mechanical properties are enhanced with increasing sintering contact points per unit volume and the bonding intensity. Some analytical models have been developed based on the assumption of affine deformation of the fibre network (Clyne et al., 2005; Markaki and Clyne, 2005; Picu, 2011; Tsarouchas and Markaki, 2011).

The relative density can significantly affect the strength and stiffness of porous materials (Gibson and Ashby, 1997; Chen et al., 1999; Jin et al., 2013; Won et al., 2013; Zhu et al., 2001, 2000, 1997); however, it is difficult to control the relative density in the manufacturing process. Finite element method (FEM) which was originally developed for solving solid mechanics problems offers a means to probe the mechanical properties of intricate stochastic fibrous materials by controlling the relative density and other key parameters in the model. In addition, optimized design of complex porous materials can be realized by finite element method. In Finite Element (FE) modelling, beams are mostly utilized to represent fibres and the way to treat the connections between the beams/fibres is crucial. A comprehensive study on the modelling of stochastic fibrous materials by mathematical treatment, for instance, the probability and distribution, can be found in reference (Sampson, 2008); however, the connection between fibres was not taken into consideration. Sastry and co-workers (Sastry et al., 2001; Wang et al., 2000; Wang and Sastry, 2000) proposed a technique for modelling fibre–fibre joints in which connection realized by a torsion spring can be regarded as flexible; however, the mechanical properties of fibrous networks with flexible bonding were not given. It is suggested that the connectivity between fibres cannot be adequately described by single connection points in the beam modelling (Wang and Sastry, 2000).

In this study, we have incorporated the density of intersections (or connections) into our model. This is important because the density of intersections is directly related to the relative density in stochastic fibrous materials. In our fibre network model, there is no fibre entanglement which is commonly found in woven fabrics (Grishanov et al., 2012). It is generally recognised that the macroscopic stresses and strains can be determined by the microscopic stresses and strains over a representative volume element (RVE). Hill (1963) proposed that a representative 'cell unit' (or a representative volume element) (RVE) can be a full-scale model to significantly reduce the computation complexity.

Traditionally the yielding of a material is defined according to the von Mises equivalent stress versus strain curve; however, it cannot be used to describe the yielding of a porous material when it is subjected to hydrostatic loading as the von Mises criterion is only based on the distortional part of the stored strain energy density. Some researchers have put forward the characteristic stress and strain which combine the hydrostatic energy density and deviatoric energy density to probe the yielding of two-dimensional isotropic honeycombs (Chen et al., 1999; Chen and Lu, 2000), two-dimensional anisotropic cellular materials (Alkhader and Vural, 2009) and three-dimensional transversely isotropic foams (Ayyagari and Vural, 2015; Zhao et al., 2013). The deduction of characteristic stress and strain is based on the total stored strain energy density and is different from those phenomenological yield criterions, for instance, a shape parameter needs to be given to describe the mean-effective stress (Deshpande and Fleck, 2000).

It has been suggested that there exists a significant difference between different types of cellular materials, such as foams and honeycombs, and fibre network materials (Markaki and Clyne, 2003; Qiao et al., 2009; Zhao et al., 2013). It is crucial to build quantitative mechanical models to reveal the mechanical behaviour of stochastic fibre network materials. Due to the computation limitation, we have used a RVE to represent a whole fibre network material. The RVE thus must be periodic. It has been shown that periodic boundary conditions are more suitable than either mixed boundary conditions or prescribed displacement boundary conditions (Chen et al., 1999; Zhu et al., 2000, 2001). To begin with, a three-dimensional periodic beam network model for stochastic fibre network materials has been constructed. We have introduced a novel method to
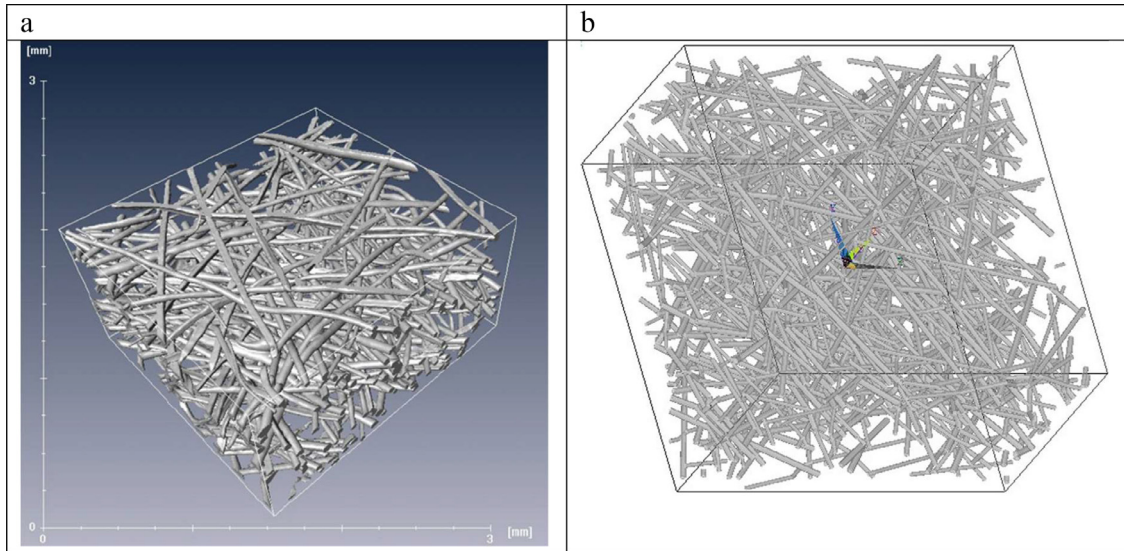
Fig. 1. The architecture of the stochastic fibre network materials: (a) 3-D reconstruction from the X-ray computed tomography (Tsarouchas and Markaki, 2011); (b) 3-D periodic random beam-network model.

deal with the connections between the fibres, in which additional beams are inserted to represent the connections (i.e. flexible cross-linkers). The elastic properties of the stochastic fibre network materials are investigated before proceeding to reveal their plastic behaviour. A scalar measure of characteristic stress and strain is utilized based on the total stored strain energy density irrespective of loading path. The objective has been to investigate the yield surface of 3D stochastic fibre network materials under multi-axial loadings and the dependence of elastic-plastic behaviour on the density of cross-linkers (i.e. connections) and the relative density of the fibre network materials.

2. Simulation methods

2.1. Construction of three-dimensional stochastic periodic beam-network model

X-ray tomography has been utilized to extract the exact architectural characteristics from the very complicated porous fibre-network material and the data are used to reconstruct the geometrical model for this material (Clyne et al., 2005; Tsarouchas and Markaki, 2011) as shown in Fig. 1a; however, this technique is very computationally challenging. Finite element models are an attractive approach to constructing the complex stochastic fibre-network structure based on fundamental geometrical parameters extracted from the X-ray computed tomography. In this paper, we have developed a code to construct a three-dimensional periodic stochastic beam-network model, as shown in Fig. 1b, which shows a close similarity with the geometry from X-ray tomography.

In our study, the model generated is a three-dimensional stochastic fibre network structure with periodicity. In addition, we have properly incorporated the deformation mechanisms of the cross-linkers into the stochastic fibre-network by inserting additional beam elements between the intersected fibres as shown in Fig. 2. The establishment of the three-dimensional beam-network model is deduced progressively with the two-dimensional coordinates being considered first. A representative volume element (RVE) is adopted due to the computational limitation. The RVE must be periodic to meet the continuity and equilibrium between any two neighbouring RVEs. Thus, to construct a periodic stochastic fibre-network model in a two dimensional (i.e. the x-y plane) square domain of a side length $w = 1.0$, the x and y coordinates of the fibre centre, the fibre length L, diameter d and orientation θ are all specified by independent random numbers which are generated by the computer and ranged from 0 to 1.0. Both of the x and y coordinates are controlled to be in the range from 0.0 to 1.0, the fibre length is from 0.8 to 1.2 (the mean length is $\bar{L} = 1.0$), the diameter is from 0.0086 to 0.0136 (the mean diameter is $\bar{d} = 0.111$), and the orientation is from 0 to π. As shown in Fig. 3, the parts of a fibre outside the square domain $w \times w$ are shifted into the domain by translating w in the x or y direction so that the RVE model is periodic in these directions.

The three-dimensional model is based on the two-dimensional one, but it requires a more complex design in terms of the intersections between fibres. All the information of the intersections between any two fibres is carried by the two-dimensional model, but there is a processing sequence of the fibres when we consider the growth in the out-of-plane dimension. By piling up the fibres one by one until N fibres are layered in the model, we construct the stochastic fibre-network model which has a significant structural component in the third dimension. In real fibre network materials, each fibre is bent away to connect the neighbouring fibres. For simplicity, polylines are used to represent the bent fibres in the 3D periodical stochastic fibre-network, in which the density of cross-linkers (i.e. connections or intersections between
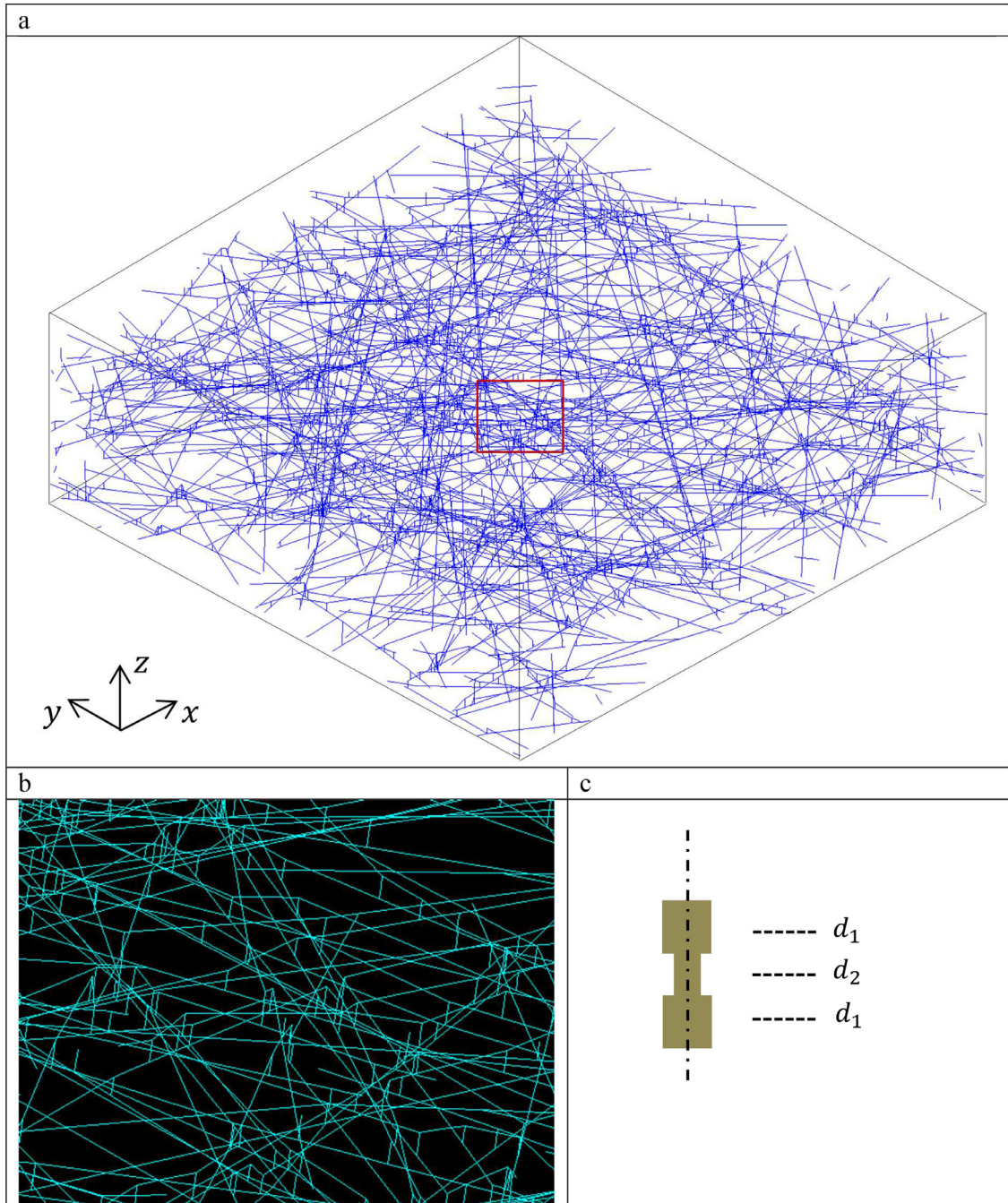
Fig. 2. Three-dimensional stochastic fibre-network model with periodicity: (a) the isometric view of the stochastic fibre-network model where the fibres are represented by the polylines; (b) the cross-linkers in the fibre-network represented by additional beam elements inserted between the intersected fibres; (c) the cross-sectional diameters of the inserted beam elements.

fibres) is incorporated. In our model with polylines, except for the two free endpoints of each fibre (polyline), all the vertices are used to represent for the intersection points (i.e. the cross-linkers). The number of intersections of a fibre with those below it is controllable and adjustable according to the nature of the actual material, thus we define this number as the density of cross-linkers, $N_c = \bar{L}/l_c$, where l_c is the mean distance between any two neighbouring intersection points of a fibre with those below it, and $\bar{L}$ is the mean length of the fibres in the model ($\bar{L} = 1.0 = 90\bar{d}$). Before going on to the detailed setup of the polyline model, it should be noted that the smoothly curved line model could be better in describing the real structure; however, a very large number of solid elements instead of beam elements may have to be used to model the real
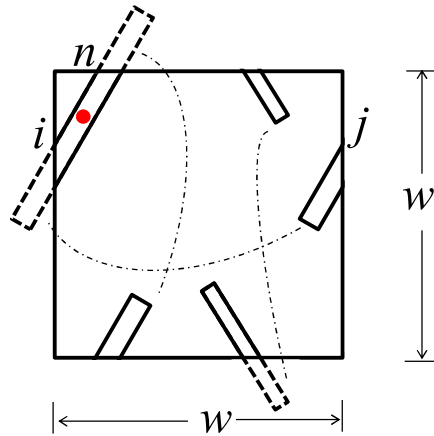
Fig. 3. Operations to generate each of the fibres in the 2D domain ($w \times w$) of a periodic representative volume element (RVE).
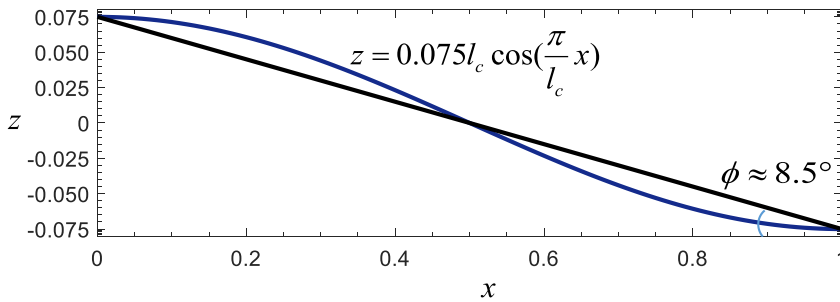

Fig. 4. A cosine-type curve cantilever beam and an inclined straight cantilever beam with an angle of 8.5° with respect to the x-y plane. Their lengths are close to l_c, with the former at 1.0137 l_c and the latter at 1.0111 l_c. The x and z axes are normalized by l_c.

Table 1
Comparison between the reaction solutions of curved cantilever beam and inclined straight cantilever beam subjected to individual displacements u_i or rotations θ_i of 0.001.

		FX	FY	FZ	MX	MY	MZ
$u_x = 0.001$	Curved	0.51896	0.16312e-10	0.18808e-35	0.85954e-20	0.13294e-17	0.77844e-01
	Straight	0.57433	0.18105e-10	0.14494e-41	0.37940e-18	0.14296e-17	0.86150e-01
$u_y = 0.001$	Curved	0.56046e-12	0.15252e-01	0.48148e-33	0.30167e-19	0.26014e-18	0.15252e-01
	Straight	0.19490e-11	0.15258e-01	0.65380e-41	0.67197e-19	0.25320e-18	0.15258e-01
$u_z = 0.001$	Curved	0.46952e-20	0.12690e-17	0.14848e-01	0.22273e-02	0.14848e-01	0.25456e-18
	Straight	0.85055e-28	0.56703e-27	0.14924e-01	0.22386e-02	0.14924e-01	0.25751e-18
$\theta_x = 0.001$	Curved	0.85944e-20	0.23228e-17	0.12145e-11	0.39764e-02	0.77691e-12	0.21869e-20
	Straight	0.34123e-18	0.22749e-17	0.79215e-12	0.39819e-02	0.45453e-12	0.12026e-19
$\theta_y = 0.001$	Curved	0.40755e-22	0.11015e-19	0.64177e-12	0.39099e-12	0.50962e-02	0.87023e-19
	Straight	0.65769e-19	0.43846e-18	0.42779e-11	0.10342e-12	0.51164e-02	0.86037e-19
$\theta_z = 0.001$	Curved	0.24524e-12	0.76302e-12	0.11575e-32	0.32461e-21	0.87733e-19	0.51373e-02
	Straight	0.10293e-11	0.14921e-11	0.18925e-32	0.13047e-19	0.86981e-19	0.51502e-02

structure, which would lead to enormous computational complexity even when the number of fibres is only 10 in the model. Alternatively, polylines could be used to represent the curved lines. We examined 10000 segments in our polyline model, the mean angle of the inclined segments with the x-y plane, $\bar{\phi}$, is around 8.5°, and the relative error with 95% confidence associated with this mean angle is below 5%. The mechanical behaviour of a curved cantilever beam expressed by the trigonometric function $z = 0.075l_c \cos(\frac{\pi}{l_c}x)$ is compared with that of an inclined straight cantilever beam with the same span of l_c, as shown in Fig. 4, when their left ends are fully fixed and six different loadings are separately applied to their free right ends. The element type utilized in the simulation of both the beams is BEAM189 and the reaction solutions are presented in Table 1. Note that the simplification by using polylines to represent the curved fibres does not cause significant error in predicting the performance of the fibre network model, moreover, the innovative modelling method optimises the simulation with both efficiency and accuracy.

In the numerical model, we have introduced an innovative way to incorporate the deformation mechanisms of the cross-linkers into the computer simulation. As shown in Fig. 2b, an additional beam with sections of different diameters is inserted
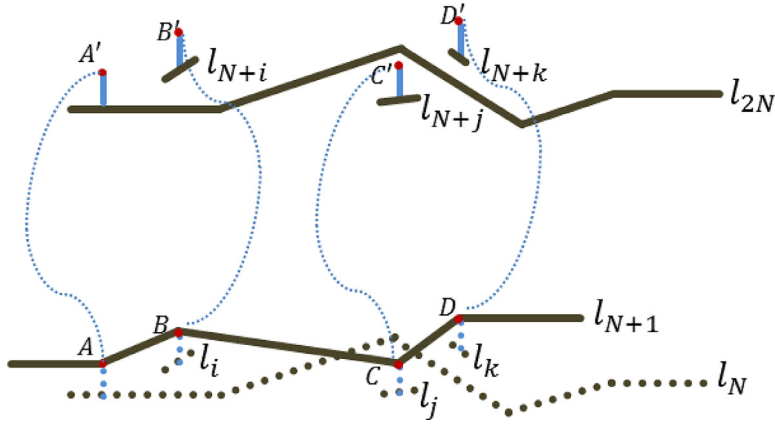
Fig. 5. Schematic diagram to show the periodicity in the out-of-plane direction.

into the intersection of two connected fibres in the thickness direction (i.e. the z direction). The length of the inserted beam is set as $\frac{0.95}{2}(d_i + d_j)$, where d_i and d_j are the diameters of the two intersected fibres. As the strength of the stochastic fibre network materials is sensitive to the cross-sectional diameter of the inserted beam, in the study of this paper, the inserted beam has been divided into three sections with different cross-sectional diameters (as shown in Fig. 2c). The dimensions of the inserted beam can affect the stiffness and strength of the fibre network structure, especially in the z direction which is parallel to the axial direction of the inserted beam. In an industrial process, if two metal fibres are partially overlapped because of, for instance, high temperature, the middle part of the inserted beam is usually thinner than the two end parts. If two fibres intersect at a right angle, the minimum diameter of the intersected part (which is in the middle of the inserted beam) is $d_{min} = 2R\sqrt{1 - 0.9^2} = 0.436\bar{d}$. In this study, the diameters of the inserted segmented beams are $d_1 = \bar{d}$ and $d_2 = \frac{1}{2}\bar{d}$. The dependence of plastic behaviour of the fibre network materials on the dimension of the cross-linker will be elucidated in Section 5. The way to achieve periodicity in the z direction for a fibre-network model with N complete fibres is shown in Fig. 5. After having built up a stochastic three-dimensional fibre-network model with N complete fibres, another N fibres are continuously put up in the z direction, whose x and y coordinates are identical to those of the previous N fibres correspondingly. Ideally the shape of the $(i+N)$th fibre is the same as that of the ith fibre when N is sufficiently large. When taking the top layer fibre-network model with N complete fibres for simulation, there are some isolated cross-linkers (i.e. inserted beam elements) indicated by the blue dotted lines. These isolated cross-linkers are moved up and the out-of-plane periodic boundary conditions are applied on their nodes.

The relative density is a key parameter to elucidate the mechanical behaviour of porous materials including fibre network materials (Jin et al., 2013; Zhu et al., 2001, 2000, 1997). In our study, we have conducted dimensional analysis to reveal the relationship between the yield strength and relative density of the stochastic fibre network materials as detailed in Section 4. By calculating the average distance between the constrained top and bottom nodes in the z direction, the thickness t of the fibre-network model is obtained. Based on the thickness, the relative density of the fibre network materials is specified by:

$$\rho = \frac{\sum_{i=1}^{N} L_i \times (\frac{1}{4}\pi \times d_i^2)}{w \times w \times t} \tag{1}$$

where $w = 1.0$, L_i are the fibre lengths (ranging from 0.8 to 1.2), N is the number of complete fibres in the periodic RVE model and d_i are the circular cross-sectional diameters (the diameter is different for different fibres from 0.0086 to 0.0136). It is not surprising that the relative density of the stochastic fibre-network materials increases with a rise in the density of cross-linkers (i.e. $N_c = \bar{L}/l_c$) based on our three-dimensional beam model developed in this study. To obtain more intersections or cross-linkers with other fibres, each fibre has to drop down so as to connect with more fibres below. This consequently reduces the thickness of the structure and thus increases the relative density. As shown in Fig. 6, the relative density of the fibre-network materials is linearly related to the density of the cross-linkers by $\rho = 0.8 \times 10^{-2}\bar{L}/l_c = 0.72\bar{d}/l_c$, where $\bar{L} = 1.0$ is the mean fibre length, $\bar{d} = 0.0111$ is the mean fibre diameter, and l_c is the mean distance between two neighbouring intersections of a fibre with those below it.

2.2. Mesh and boundary conditions

The fibre-network model is partitioned into a large number of 3-node beam elements (ANSYS element type: BEAM 189) with a circular cross-section. This element type is based on the Timoshenko beam theory and the shear deformation effect is included. The solid fibres are assumed to be an isotropic bilinear material with Young's modulus $E_s = 210$ GPa, Poisson ratio $\nu_s = 0.3$, yield strength $\sigma_s = 290$ MPa and the hardening gradient $E_t = 4.2$ GPa. The material properties of the flexible cross-linkers, which were implemented by additional inserted beams, are assumed to be the same as those of the fibres.
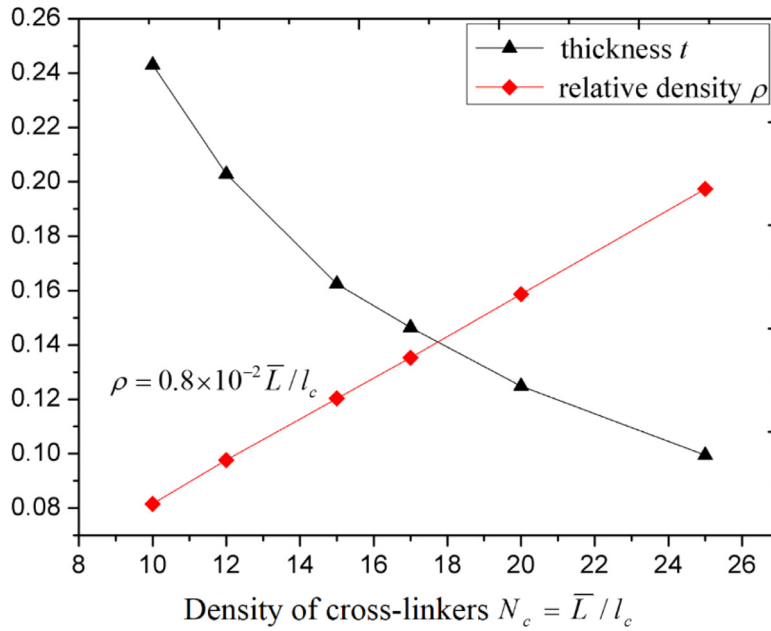
$$\rho = 0.8 \times 10^{-2}\, \overline{L}/l_c$$

Fig. 6. Effects of the density of cross-linkers on the thickness and relative density of stochastic fibre-network materials.

Table 2
Statistics of the relative density and normalized Young's modulus in the x direction over 20 stochastic periodic models with the number of complete fibres $N = 75$, 100, 150, 200, 400, and with fixed density of cross-linkers at $\overline{L}/l_c = 10$, and the mean slenderness ratio $\overline{L}/\overline{d} = 90$.

	Relative density		Normalized Young's modulus	
	Mean	Std. deviation	Mean	Std. deviation
$N = 75$	0.0819839	0.0039362	9.241E-03	1.870E-03
$N = 100$	0.0824473	0.0018767	9.185E-03	1.323E-03
$N = 150$	0.0818737	0.0017731	9.351E-03	1.252E-03
$N = 200$	0.0816073	0.0013956	9.285E-03	0.615E-03
$N = 400$	0.0816904	0.0012343	9.301E-03	0.607E-03

It is very important to choose appropriate boundary conditions in the numerical simulation. Periodic boundary conditions are in general more suitable than mixed boundary conditions and prescribed displacement boundary conditions to analyse the mechanical properties of a periodic RVE (Chen et al., 1999; Zhu et al., 2000, 2001). It is assumed that the corresponding nodes on the opposite edge of the mesh have the same expansion in the normal direction, the same displacement in other directions, and the same rotations in all directions. For uniaxial loading in the x direction as an example, a tensile or compressive displacement/strain in the x direction is applied to the corresponding reference nodes on the opposite boundaries. For biaxial or triaxial loading, proportional strains are applied on the corresponding reference nodes in two or three directions simultaneously, for instance, $\varepsilon_x : \varepsilon_y = 1 : 1$, $\varepsilon_x : \varepsilon_z = -1 : 1$, $\varepsilon_x : \varepsilon_y : \varepsilon_z = 1 : 1 : 2$.

It is necessary to determine the number of complete fibres N in the RVE as N should be sufficient so that the mechanical properties obtained from the stochastic beam-network model are stable and correct. A mesh sensitivity study has been performed by changing the total number of complete fibres N for models having a fixed density of cross-linkers $\overline{L}/l_c = 10$. Twenty stochastic models are investigated for each different number of complete fibres $N = 75$, 100, 150, 200, 400. It is noted that the thickness of the periodic fibre network model increases as the number of complete fibres increases. Each stochastic periodic fibre-network model is generated using a different list of random numbers, and has the same diameter range, $d \in (0.0086, 0.0136)$. The statistical results of the Young's modulus in the x direction and the relative density of the fibre-network materials are obtained and shown in Table 2, where the Young's modulus of the fibre-network materials is normalised by the Young's modulus of the solid material, E_s. The simulation results are obtained by using the finite element solver of ANSYS APDL software. As seen in Table 2, the mean densities and Young's moduli in the x direction are almost the same for all the different cases, $N = 75$, 100, 150, 200, 400. In contrast, the standard deviations for both the Young's modulus and the relative density of the fibre-network materials are trending downward, i.e., the larger the number of complete fibres, the smaller will be the standard deviation. Theoretically, the reaction force of double layers should be twice as large as that of single layer (i.e., $N = 150$ vs. $N = 75$, $N = 200$ vs. $N = 100...$) when all the other conditions are completely the same. The ratios of the corresponding reaction forces are listed in Table 3, and the results are the mean

Table 3
The mean ratio of paired reaction forces over twenty stochastic samples.

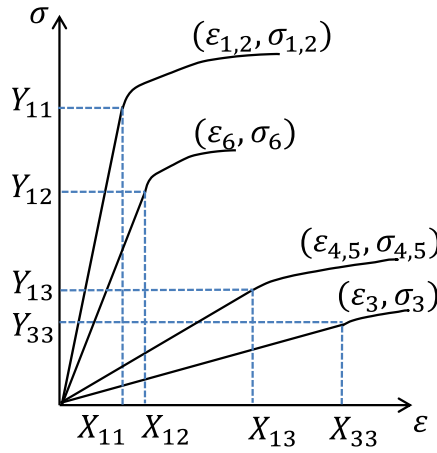|	N150/N75	N200/N100	N400/N200
Mean Ratio	2.107841	2.060466	2.020708

Fig. 7. The elastic-plastic response of transversely isotropic materials under uniaxial loading and pure shearing.

values of twenty paired stochastic models. It is worth noting that when the number of complete fibres increases, the ratio of the reaction force of two layers to that of one layer approaches 2.0. When $N = 200$, the standard deviations of the relative density, the Young's modulus in the x direction and the reaction force are all very small. Also, with the consideration of computational efficiency, the finite element results presented below are the mean results over twenty stochastic models having the number of complete fibres fixed at $N = 200$. The relative error with 95% confidence interval is 0.75% for relative density and 2.9% for Young's modulus.

3. Elasto-plastic behaviour

One of the significant features incorporated into our three-dimensional beam-network model is the anisotropic elasticity of the fibre networks. It is shown that the mean values of Young's modulus and the Poisson's ratio for 20 models are almost identical in the x and y directions, which suggests that the stochastic fibre network materials are transversely isotropic (i.e. isotropic in the x-y plane).

3.1. Characteristic stress and strain

Chen and Lu (2000) introduced characteristic stress and strain for isotropic foam, based on which, a yield criterion has been developed by hypothesizing that the yielding is driven by the total stored strain energy density, including the hydrostatic and deviatoric parts. Uniaxial response of a transversely isotropic material ($E_1 = E_2$) can be schematically represented by the stress-strain graphs in Fig. 7. To obtain a scalar measure of the strain energy density independent of the loading directions, the normalized strain energy density can be written as,

$$\bar{W} = \frac{1}{2}(\bar{\sigma}_1\bar{\varepsilon}_1 + \bar{\sigma}_2\bar{\varepsilon}_2 + \bar{\sigma}_3\bar{\varepsilon}_3 + \bar{\sigma}_4\bar{\varepsilon}_4 + \bar{\sigma}_5\bar{\varepsilon}_5 + \bar{\sigma}_6\bar{\varepsilon}_6) \tag{2}$$

where $\bar{\sigma}_1, \bar{\sigma}_2, \bar{\sigma}_3, \bar{\sigma}_4, \bar{\sigma}_5, \bar{\sigma}_6$ and $\bar{\varepsilon}_1, \bar{\varepsilon}_2, \bar{\varepsilon}_3, \bar{\varepsilon}_4, \bar{\varepsilon}_5, \bar{\varepsilon}_6$ are the normalized stresses and strains and can be expressed as $\bar{\sigma}_1 = \sigma_1/Y_{11}$, $\bar{\varepsilon}_1 = \varepsilon_1/X_{11}$, $\bar{\sigma}_2 = \sigma_2/Y_{11}$, $\bar{\varepsilon}_2 = \varepsilon_2/X_{11}$, $\bar{\sigma}_3 = \sigma_3/Y_{33}$, $\bar{\varepsilon}_3 = \varepsilon_3/X_{33}$, $\bar{\sigma}_4 = \sigma_4/Y_{13}$, $\bar{\varepsilon}_4 = \varepsilon_4/X_{13}$, $\bar{\sigma}_5 = \sigma_5/Y_{13}$, $\bar{\varepsilon}_5 = \varepsilon_5/X_{13}$, $\bar{\sigma}_6 = \sigma_6/Y_{12}$, $\bar{\varepsilon}_6 = \varepsilon_6/X_{12}$, where $Y_{11}, Y_{33}, X_{11}, X_{33}$ are the yield stresses and strains along the x and z directions for the transversely isotropic fibre-network materials subjected to uniaxial loadings, and $Y_{13}, Y_{12}, X_{13}, X_{12}$ are the shear yield stresses and strains along the 1-3 and 1-2 directions as shown in Fig. 7.

By scaling back all the normalized components of the stress and strain tensors, the characteristic stress and strain are independent of the loading path, and given as,

$$\hat{\sigma}^2 = \hat{\sigma}_e^2 + \kappa^2\hat{\sigma}_m^2 \tag{3}$$

$$\hat{\varepsilon}^2 = \hat{\varepsilon}_e^2 + \frac{\hat{\varepsilon}_v^2}{\kappa^2} \tag{4}$$

Table 4
Elastic properties and yield strengths (MPa) of the stochastic fibre-network materials with a relative density $\rho = 8.16\%$, a density of cross-linkers $\bar{L}/l_c = 10$, a mean fibre slenderness ratio $\bar{L}/\bar{d} = 90$ and total number of complete fibres $N = 200$.

Y_{11}	X_{11}	Y_{33}	X_{33}	Y_{13}	X_{13}	Y_{12}	X_{12}	E_1	E_3	v_{12}	v_{31}
3.022	1.889E-3	7.194E-2	2.959E-2	1.751E-1	7.859E-3	1.930	1.605E-3	1.975E3	3.184	2.954E-1	4.743E-3

where $\kappa^2 = \frac{\bar{E}}{\bar{K}}$, $\bar{E} = \frac{9}{6+2v_{12}+2v_{31}(\frac{Y_{11}}{Y_{33}}+\frac{X_{33}}{X_{11}})}$, and $\bar{K} = \frac{1}{3-2v_{12}-2v_{31}(\frac{Y_{11}}{Y_{33}}+\frac{X_{33}}{X_{11}})}$. $\hat{\sigma}_e$ and $\hat{\varepsilon}_e$ are the conjugate effective stress and strain derived from the deviatoric energy density, and $\hat{\sigma}_m$ and $\hat{\varepsilon}_v$ are the mean stress and volumetric strain derived from the hydrostatic energy density. The more detailed derivation can be found in reference (Zhao et al., 2013). In the elastic regime, the characteristic stress and strain satisfy $\hat{\sigma} = \hat{E}\hat{\varepsilon}$, such that

$$\hat{E} = \bar{E}E_1 \tag{5}$$

The introduction of the scalar measures of the characteristic stress and strain contributes to revealing the elastic response of transversely isotropic materials under multiaxial loadings, in which all the characteristic stress and strain curves collapse along a master line whose slope is $\hat{E}$. Note that the characteristic stress and strain carry the information on stiffness and strength anisotropy, such as Y_{11}, Y_{33}, X_{11}, X_{33}, Y_{13}, Y_{12}, X_{13}, X_{12}, E_1, E_3, v_{12}, and v_{31} which can be obtained from just the elastic-plastic response of the uniaxial loadings in the x and z directions and pure shearing along the 1-3 and 1-2 directions. The elastic properties and yield strengths (MPa) of the stochastic fibre-network materials with a relative density $\rho = 8.16\%$ are extracted from uniaxial tension and pure shearing by FE simulations, and are listed in Table 4. Johnson's apparent elastic limit has been used to determine the yield stresses, i.e., Y_{11}, Y_{33}, Y_{13}, Y_{12}, and their corresponding strains, i.e., X_{11}, X_{33}, X_{13}, X_{12}. The yield strength (i.e. Y_{11}, Y_{33}, Y_{13} or Y_{12}) is taken as the stress at the point on the stress-strain curve at which the tangent gradient is 50% of the initial gradient (i.e. the Young's modulus or shear modulus) of uniaxial loading or pure shearing (Johnson, 1918).

3.2. Yield strength and yield surface

The homogenized total strain energy density $\hat{W}$ obtained by scaling back the normalized stresses and strains based on the strength and stiffness only in the x direction can be rewritten as

$$\hat{W} = \frac{1}{2}\left(\sigma_1\varepsilon_1 + \sigma_2\varepsilon_2 + \left(\frac{Y_{11}}{Y_{33}}\frac{X_{11}}{X_{33}}\right)\sigma_3\varepsilon_3 + \left(\frac{Y_{11}}{Y_{13}}\frac{X_{11}}{X_{13}}\right)\sigma_4\varepsilon_4 + \left(\frac{Y_{11}}{Y_{13}}\frac{X_{11}}{X_{13}}\right)\sigma_5\varepsilon_5 + \left(\frac{Y_{11}}{Y_{12}}\frac{X_{11}}{X_{12}}\right)\sigma_6\varepsilon_6\right) \tag{6}$$

It is hypothesized that yielding of the stochastic fibre network structure occurs when the homogenized total strain energy density $\hat{W}$ reaches a critical value. Under the stress state of uniaxial loading in the x direction, yielding occurs when $\sigma_1 = Y_{11}$, thus $\hat{\sigma}_m = \frac{Y_{11}}{3}$; $\hat{\sigma}_e = Y_{11}$. Therefore, the yield criterion of the stochastic fibre-network materials under any arbitrary state of stresses is given as

$$\hat{\sigma}_e^2 + \kappa^2\hat{\sigma}_m^2 = \left(1 + \frac{\kappa^2}{9}\right)Y_{11}^2 \tag{7}$$

From Eq. (7) it can be seen that the scaling back direction can affect the size of the yield surface (i.e. the amplitude of the right hand side of Eq. (7)) in the space of the mean normal stress versus the effective stress. To give a more general yield criterion, the mean and effective stresses are normalized by Y_{11}. Thus, the yield criterion of the stochastic fibre network materials becomes,

$$\bar{\sigma}_e^2 + \kappa^2\bar{\sigma}_m^2 = \left(1 + \frac{\kappa^2}{9}\right) \tag{8}$$

where $\bar{\sigma}_e = \hat{\sigma}_e/Y_{11}$ and $\bar{\sigma}_m = \hat{\sigma}_m/Y_{11}$. The elastic constants and yield strength of the stochastic fibre-network materials with a relative density $\rho = 8.16\%$ are obtained from FE simulation, and are used in Eq. (8) to plot the yield surface in the space of the normalised mean normal stress versus the effective stress (in MPa), as shown in Fig. 8.

3.2.1. Characteristic strain offset value
Characteristic stress-strain curves can be used to determine the yield point for stochastic fibre network materials in a unique manner even under different states of stresses as all the characteristic stress-strain curves fall on the same line before yielding. The traditional yield strain for solid mild steel is 0.2% in experimental studies (Chen et al., 1999; Zhao et al., 2013). In this study, the yield strain is taken as the strain at the point on the stress-strain curve of uniaxial loading in the x direction at which the tangent gradient is 50% the initial gradient (i.e. the initial Young's modulus E_1). Thus, the yield strain is 0.136% for stochastic fibre-network materials with a relative density $\rho = 8.16\%$. Note that the characteristic yield strain or stress is independent of the state of the stresses, thus the value is the same as those obtained by using the yield points of either the uniaxial loading in the z direction or pure shearing along the 1-3 or 1-2 directions.
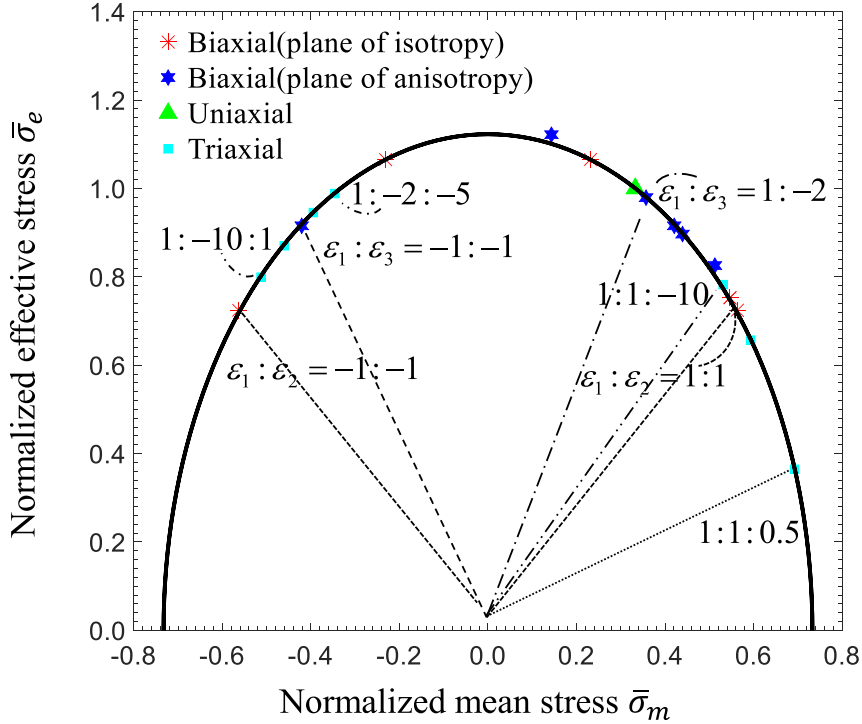
Fig. 8. The yield surface of transversely isotropic stochastic fibre network materials obtained from FE simulation under multiaxial loadings.

3.2.2. Multiaxial normal stress states

With the energy-based yield criterion, the yield function can be fully calibrated in terms of the uniaxial tension (or compression) response in the x or z direction, or by pure shearing along the 1-3 or 1-2 directions instead of complex multiaxial loading responses.

The characteristic stress- strain curves from the FE simulations for various biaxial strain paths in both the plane of isotropy and the plane of anisotropy are plotted in Fig. 9. All the data points on the graphs are from the same stochastic fibre network structure with the relative density $\rho = 8.16\%$, the density of cross-linkers $\bar{L}/l_c = 10$, the fibre aspect ratio $\bar{L}/\bar{d} = 90$ and the number of fibres $N = 200$. As can be seen from Fig. 9, for biaxial loadings in both the plane of isotropy (x-y plane) and plane of anisotropy (x-z plane), all the characteristic stress-strain curves collapse on a single master line in the elastic regime. Interestingly, the stochastic fibre network structure model shows identical properties under small amplitude ($\varepsilon \leq 0.6\%$) uniaxial tension and compression in the x and z directions. In addition, when this network is subjected to equi-biaxial tension in the plane of isotropy ($\varepsilon_x : \varepsilon_y = 1 : 1$), the response is the same as that of equi-biaxial compression ($\varepsilon_x : \varepsilon_y = -1 : -1$). Also, this conclusion is applicable in the plane of anisotropy. The model developed in this study therefore is pressure independent under small strain deformation. Under large deformation, the responses under tension and compression are certainly different because of geometrical nonlinearity and different dominant failure mechanisms (e.g. fracture in tension and buckling under compression). This paper is therefore focused on the small strain deformation without out buckling. In the plane of anisotropy for the stochastic fibre network structure, the characteristic stress-strain curves under proportional biaxial loadings, such as $\varepsilon_x : \varepsilon_z = 1 : 1$, $1 : -2$, $1: 2$, show significant similarities. It is mainly attributed to the much larger strength and stiffness in the x direction than that in the z direction. As the properties of the structure are dominated by the axial loading in the x direction in the plane of anisotropy, a slight change in loading of the z direction hardly affects the plastic response of the stochastic fibre network structure. The yield surface of transversely isotropic stochastic fibre network materials obtained from FE simulations under multiaxial loadings is plotted in Fig. 8 in the space of characteristic effective stress and mean stress. As the strength and stiffness in the z direction are smaller than those in the x or y direction, the sign of effective stress of the fibre network materials in the multiaxial loadings is always the same as that of the stress in the x or y direction rather than the z direction, e.g., $\varepsilon_x : \varepsilon_y : \varepsilon_z = 1 : 1 : -10$, $\varepsilon_x : \varepsilon_y : \varepsilon_z = 1 : -10 : 1$ as shown in Fig. 8.

3.2.3. Combined axial loading and shearing

It is noted that the presence of the shear stress component does not affect the form of the yield criterion given in Eq. (8). In the plane of isotropy (i.e. the x-y plane), we do not need to consider the effect of the shear stress on the yield surface
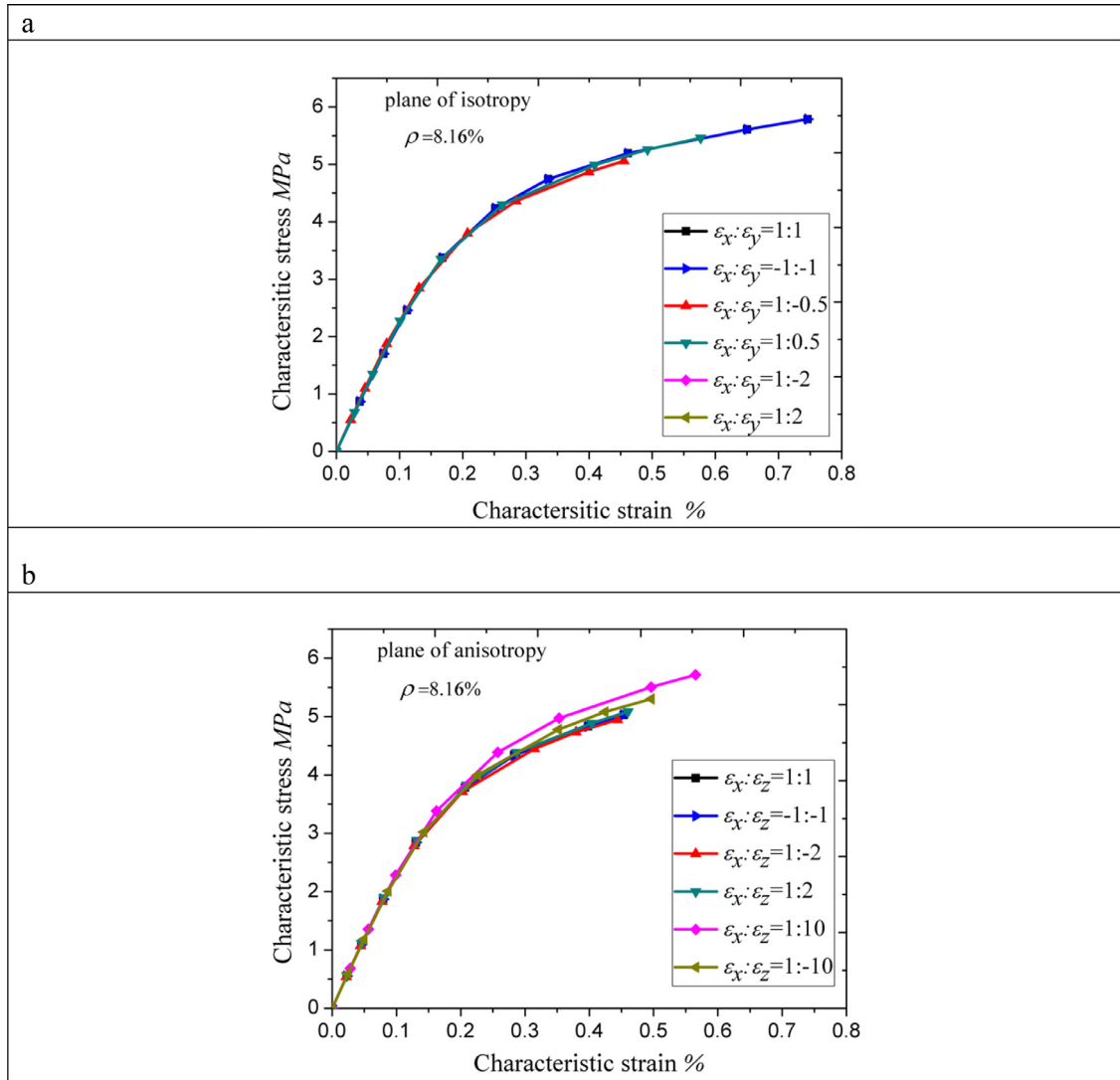
Fig. 9. Characteristic stress-strain relations under biaxial loading in the (a) plane of isotropy and (b) plane of anisotropy.

(i.e. Fig. 8) because the principal stresses in this plane can always be obtained. In the plane of anisotropy (i.e. the *x-z* or *y-z* plane), the presence of the shear stress component contributes to the amplitude of the normalised characteristic deviatoric stress in Eq. (8), thus, it reduces the size, but does not change the shape of the yield surface, as can be seen in Fig. 10 where the unit of the stress is MPa. When the shear stress is absent, the size of the yield surface in the plane of anisotropy arrives at its maximum. With the increase of the shear stress, the size of the yield surface decreases.

4. Effects of relative density on the uniaxial yield strength

The effects of the density of cross-linkers $\bar{L}/l_c$ on the elastic constants and yield strengths of random fibre-network materials can be evaluated from the relationships between the relative density of the fibre network and its stiffness and strength. The relative density can be adjusted by changing the density of cross-linkers (i.e. the number of intersections of a fibre with those below it) as the relative density of a fibre network material has a linear correlation with the density of cross-linkers (see Fig. 6).

4.1. Simulation results

In practical applications, one of the most important properties about the fibre network materials is the relationship between their yield strength and their relative density. To obtain the uniaxial yield strength, we first obtain the uniaxial tensile stress strain relationship for stochastic fibre network materials with different relative densities. The yielding is supposed to
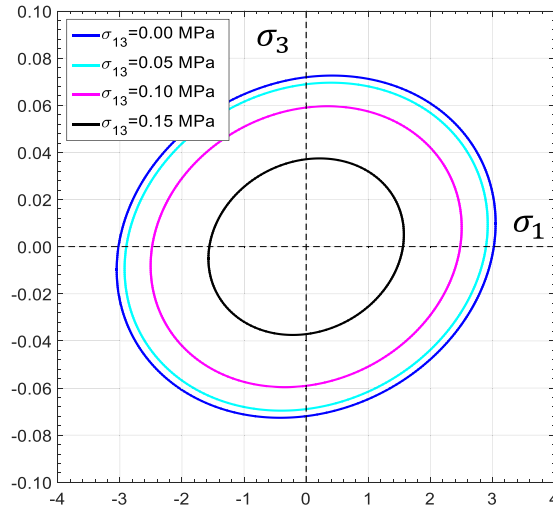
Fig. 10. Effect of shear stress on the yield surface in the plane of anisotropy.
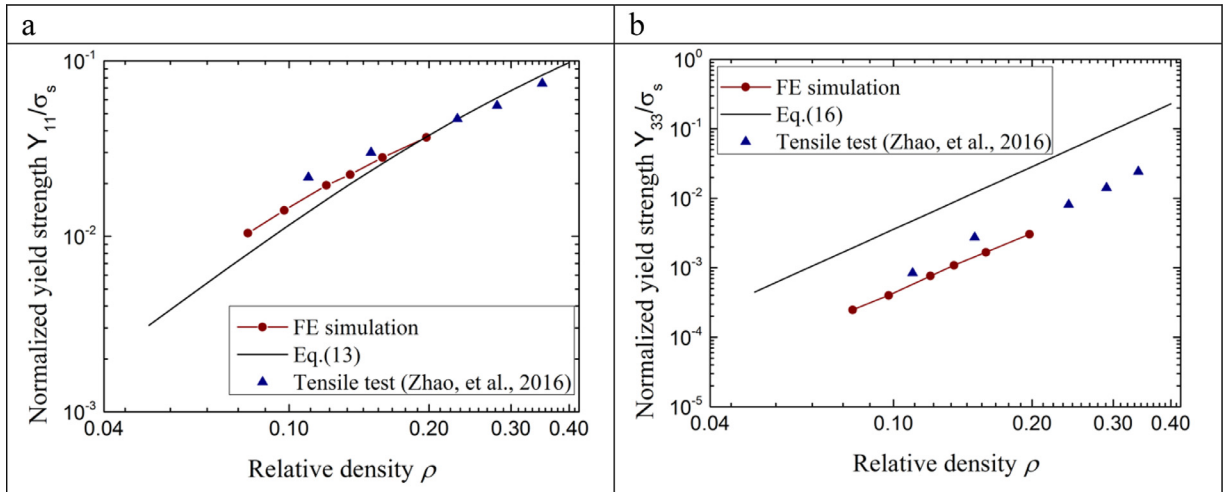

Fig. 11. The relationship between the relative density and the uniaxial yield strength of stochastic fibre network materials in the *x* direction (a) and in the *z* direction (b).

occur at the point on the uniaxial tensile stress-strain curve at which the tangent gradient is 50% of the elastic constant (i.e. the initial Young's modulus) (Johnson, 1918).

The finite element simulation results indicate that the uniaxial yield strength in the x direction is a quadratic function of the relative density of the stochastic fibre network materials when the relative density is small (i.e. $\rho \leq 0.2$), as shown in Fig. 11(a). In contrast, the uniaxial yield strength in the z direction is constantly a cubic function of the relative density, as can be seen in Fig. 11(b).

A shear deformation is enforced by imposing a pair of shear strains in transverse directions. The shear yield strength is taken as the stress at the point on the stress-strain curve where the tangent gradient is 50% of the shear modulus of pure shearing (Johnson, 1918). The effects of relative density on the shear strength of stochastic fibre network materials are shown in Fig. 12. The in-plane shear strength Y_{12} is a quadratic function of the relative density when $\rho \leq 0.2$ (see Fig. 12(a)), and it gradually becomes a linear function when $\rho \geq 0.22$ (see Eq. (13)). The out-of-plane shear strength Y_{13} of the fibre network materials is much lower than their in-plane shear strength Y_{12}. Experimental tests of MFSSs suggest that the in-plane and out-of-plane shear strengths have linear and cubic dependence upon the relative density, respectively (Zhao and Chen, 2014). The simulation of our 3-D random beam model is broadly consistant with the experimental results, especially a cubic function in the transverse direction as can be seen in Fig. 12(b).
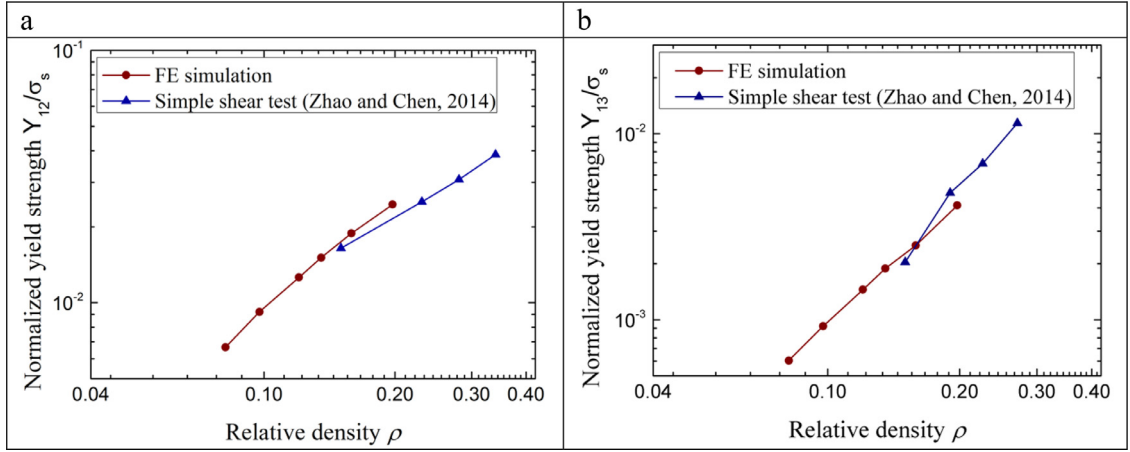
Fig. 12. The effects of relative density on the shear strength of stochastic fibre network materials: (a) in-plane shear; (b) out-of-plane shear.

4.2. Results of dimensional analysis

To perform dimensional analysis, one has to simplify and/or idealise the geometrical structure of the fibre network materials. As the stochastic fibre network materials are transversely isotropic with the properties in the x direction the same as those in the y direction, the geometrical model for dimensional analysis is simplified, as shown in Fig. 13(a). This model is periodic in all the x, y and z directions.

4.2.1. Uniaxial yield strength in the x direction

Fig. 13(b) shows the contour of von Mises stress when the low-density fibre network materials undergo uniaxial tension in the x direction. It indicates that bending and torsion are the dominant deformation mechanisms. As each segment of the fibres along the y direction can be regarded as a beam with a span of l_c and its two ends clamped, when an external force P from the intersected fibre in the x direction is transversely applied to the middle of the segment fibre/beam, the maximum bending moment and torque in the segment beam (along the y direction) can be obtained as

$$M_{max} = \frac{1}{8} P l_c; \qquad T_{max} = \frac{0.95}{2} P \bar{d} \tag{9}$$

where $\bar{d}$ is the mean diameter of the fibres, $P = 1.9 l_c \bar{d} \sigma_x$ and σ_x is the effective uniaxial tensile stress applied to the fibre network materials in the x direction. Note that the distance between the centroidal lines of two intersected fibres is taken as $0.95\bar{d}$ in the model.

The maximum von Mises stress in the segment beam (along the y direction) is related to the uniaxial tensile stress by

$$\sigma_{Mises} = \sqrt{\left(\frac{\bar{d}M_{max}}{2I}\right)^2 + 3\left(\frac{\bar{d}T_{max}}{2J}\right)^2} = \frac{4 \times 1.9 \sigma_x l_c \bar{d}}{\pi (\bar{d})^2} \sqrt{\left(\frac{0.72}{\rho}\right)^2 + 10.83} \tag{10}$$

The relationship $\rho = 0.72\bar{d}/l_c$ from Fig. 6 has been used to derive the above equation.

When the solid fibre is just about to yield, the maximum von Mises stress in the solid material of the segment beam reaches the yield strength σ_S and the corresponding stress σ_x reaches the initial uniaxial yield strength of the fibre network materials, $(Y_{11})_i$, this leads to

$$\sigma_S = \sqrt{\left(\frac{\bar{d}M_{max}}{2I}\right)^2 + 3\left(\frac{\bar{d}T_{max}}{2J}\right)^2} = \frac{4 \times 1.9 (Y_{11})_i l_c \bar{d}}{\pi (\bar{d})^2} \sqrt{\left(\frac{0.72}{\rho}\right)^2 + 10.83} \tag{11}$$

Thus, the initial uniaxial yield strength of the fibre network materials in the x direction can be obtained as a function of the relative density, and given as

$$(Y_{11})_i = \frac{0.797 \rho^2}{\sqrt{1 + 20.89 \rho^2}} \sigma_S \tag{12}$$

For a uniform beam with a circular cross-section, the full bending capacity is 1.7 times the bending moment at initial yielding, and the full torsion capacity is 1.5 times the torque at initial yielding. Thus, the uniaxial tensile strength (or yield strength) of the fibre network materials can be approximately expressed as

$$Y_{11} = 1.6(Y_{11})_i = \frac{1.275 \rho^2}{\sqrt{1 + 20.89 \rho^2}} \sigma_S \tag{13}$$
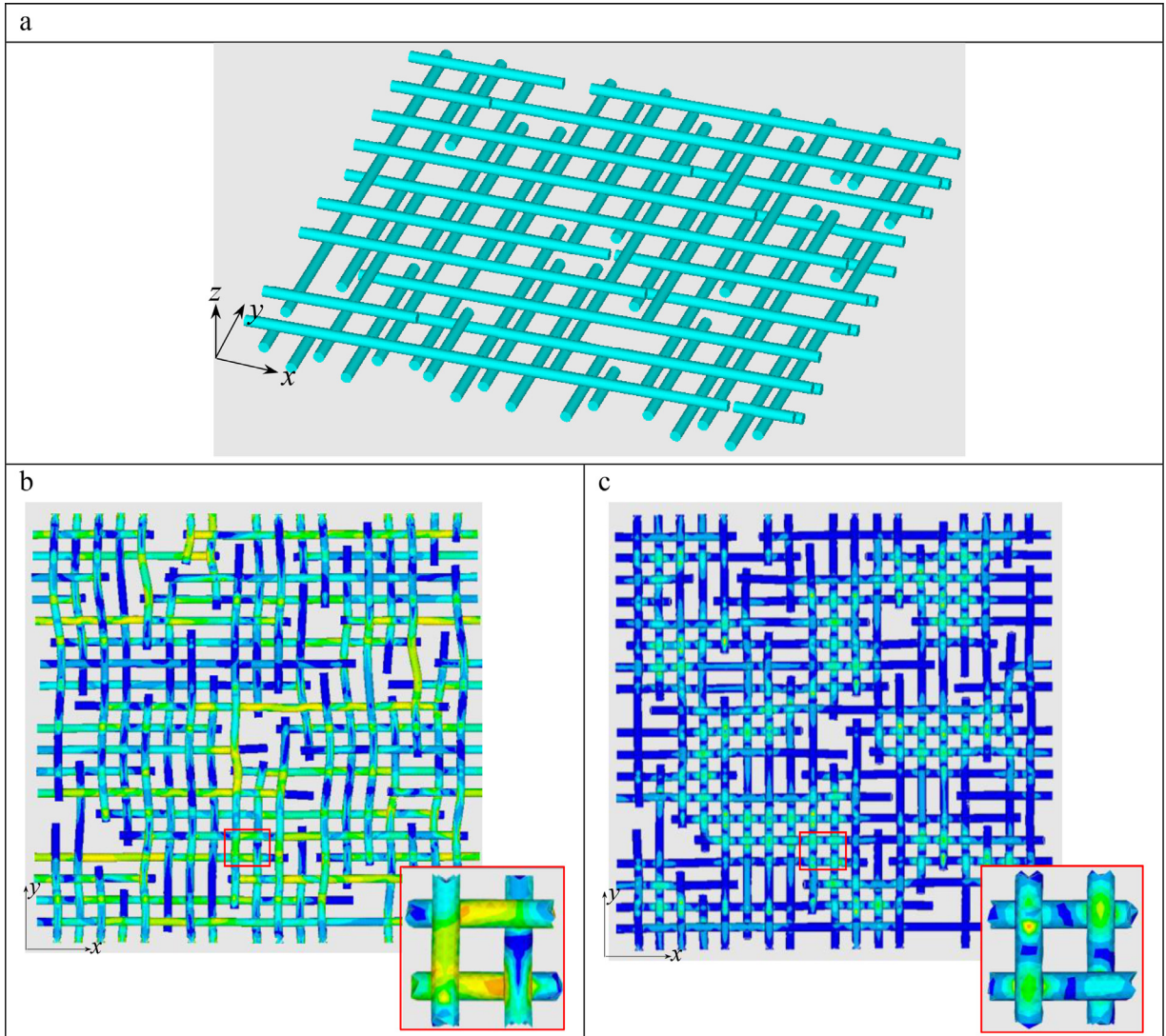
Fig. 13. The simplified schematic model of the fibre network materials for dimensional analysis.

The dimensional analysis results from Eq. (13) are presented in Fig. 11(a) for comparison with the simulation results and experimental results (Zhao et al., 2016), showing excellent agreement.

Eq. (13) suggests that when the relative density is small (i.e. $\rho \leq 0.2$), the in-plane tensile strength Y_{11} is a quadratic function of ρ; while when the relative density is large (i.e. $\rho \geq 0.22$), the denominator is dominated by the term $20.89\rho^2$ and the in-plane tensile strength Y_{11} gradually becomes a linear function of ρ.

4.2.2. Uniaxial yield strength in the z direction

In the random beam model developed in this paper, the cross-linkers (or intersections) are represented by inserted beam elements which are in parallel to the z direction. When the simplified model is stretched by a uniaxial tensile stress σ_z in the z direction, the contour of von Mises stress in the idealised fibre-network materials is shown in Fig. 13(c). As can be seen, bending is the dominant deformation mechanism.

According to the simplified model, the effective uniaxial tensile stress σ_z applied to the fibre network materials in the z direction can be related to the maximum von Mises stress in the solid fibre by

$$\sigma_{Mises} = \frac{\overline{d}M_{\max}}{2I} = \frac{\overline{d}Pl_c}{16I} = \frac{4l_c^3\sigma_z}{\pi\left(\overline{d}\right)^3} = \frac{0.475}{\rho^3}\sigma_z \tag{14}$$

When the solid fibre is just about to yield, the maximum von Mises stress in the segment beam reaches the yield strength of the solid material σ_S and the corresponding stress σ_z reaches the initial uniaxial yield strength of the fibre

network materials, $(Y_{33})_i$, leading to

$$(Y_{33})_i = 2.105\rho^3\sigma_S \tag{15}$$

As the full bending capacity of a uniform beam with a circular cross-section is 1.7 times the bending moment at initial yielding, the uniaxial tensile strength (or yield strength) of the fibre network materials in the z direction can be approximated as

$$Y_{33} = 1.7(Y_{33})_i = 3.58\rho^3\sigma_S \tag{16}$$

The dimensional analysis results from Eq. (16) are presented in Fig. 11(b) for comparison with the simulation results and experimental results (Zhao et al., 2016), confirming that the difference is just a constant factor and fibre bending is indeed the dominant deformation mechanism.

The results in Fig. 11(a) and (b) demonstrate that the above dimensional analyses obtained from a simplified model have correctly captured the main deformation mechanisms when the stochastic fibre network materials undergo uniaxial in-plane or out-of-plane tension. It is noted that the dimensional analyses assume that the relative density ρ is the same or uniform over the whole model of the fibre network materials, while in reality, the local density could be double or half the average relative density at different locations. When the fibre network materials undergo uniaxial tension in the x direction, the beam/fibre-network can be treated as a number of springs (with different stiffnesses) which are deformed partly in parallel and partly in series. As Y_{11} is proportional to ρ^2 when $\rho \leq 0.2$ and to ρ when $\rho \geq 0.22$, it is less affected by the non-uniform distribution of the relative density. When the fibre network materials undergo uniaxial tension in the z direction, the beam/fibre-network can be treated as a number of springs (with different stiffnesses) in series. As Y_{33} is proportional to ρ^3, the yield strength of the fibre-network materials is mainly dominated by the locations where the relative density is much lower than the average. That is why the dimensional analysis results are closer to the simulation results in the x direction, but much larger than those in the z direction. The strong agreement from the comparison, as shown in Fig. 11, indicates that our fibre network models are supported by experimental evidences. Jin et al. (2013) have simulated the in-plane yield behaviour of fibre network materials and suggested that the deformation mechanism of porous metal fibre sintered sheets (MFSSs) is stretching dominated. The difference between their results and our findings is attributed to the geometrical models. For a 2-D beam model, the density of cross-linkers (intersections) is certainly significantly overestimated and this tends to predict a larger in-plane yield strength Y_{11}.

5. Discussion

The stiffness and the strength of the stochastic fibre network materials in the z direction are much lower than those in the x direction as shown in Table 4, which gives rise to a significant change in the tilt of the yield surface in the plane of anisotropy (i.e. the x-z plane). The stiffness and strength in both the x and z directions are associated with the cross-linkers between any two intersected fibres, and thus are dependent upon the density of cross-linkers $\bar{L}/l_c$, which is a key feature incorporated into our fibre network model. To obtain more intersections or cross-linkers with other fibres, each fibre must drop down so as to connect with more fibres below, which consequently reduces the thickness of the structure and, consequently, increases the relative density as shown in Fig. 6. The cross-linkers are represented by inserted beams which are divided into 3 segments with the middle segment of a diameter $d_2 = \frac{1}{2}\bar{d}$ and the other two of a diameter $d_1 = \bar{d}$, as shown in Fig. 2c. This is because the minimum diameter of the intersection of two fibres intersected at a right angle is $d_{\min} = 2R\sqrt{1 - 0.9^2} = 0.436\bar{d}$. With more inserted beam elements (i.e. more cross-linkers), the strength and stiffness of the stochastic fibre network materials increase dramatically. The elastic properties and uniaxial yield strength of the stochastic fibre network materials with different relative density (or density of cross-linkers) are simulated. As can be seen from Fig. 11, with the increase of the relative density, the uniaxial yield strengths of the fibre network materials in both the x and z directions increase, and the magnitude in the x direction is always much larger than that in the z direction; however, strength anisotropy (i.e. Y_{11}/Y_{33}) becomes less obvious. The tilt angle of the yield surface in the plane of anisotropy becomes larger as the relative density increases, e.g. the tilt angle φ_2 at $\rho = 19.74\%$ is larger than φ_1 at $\rho = 12.03\%$, as shown in Fig. 14 where the unit of the stress is MPa.

The effects of the treatment for cross-linkers (i.e. the diameters d_1 and d_2 of the inserted beams) on the yield surface/strength in the plane of anisotropy for stochastic fibre network materials with $\rho = 8.16\%$ have been investigated, as shown in Fig. 15 where the unit of the stress is MPa. The first type of treatment for cross-linkers is rigid connection (i.e. the corresponding two nodes in the intersected fibres are imposed to have the same displacements, which is more like the case of the 2D model in Jin et al., 2013). In this case, the yield strengths of stochastic fibre network materials in the x and z directions are $Y_{11} = 4.174$ MPa and $Y_{33} = 0.1051$ MPa, respectivly. The treatment of rigid connection obviously results in the largest yield strengths in both the x and z directions as shown in Fig. 15, and the obtained results are certainly over-estimated. In the second case, all the inserted beams are assumed to have the same uniform diameter of $5\bar{d}$. It is certain that there is no plastic deformation in all the inserted beams in this case; however, the yield strengths in both the x and z directions are obviously smaller than those in the first case. This is because the inserted beams (i.e. cross-linkers) could still have rigid translation and rotation, which could cause the displacements of the two end nodes of the inserted beams to differ and thus reduce the stiffness and yield strength of the fibre network materials. In the third case, all the inserted beams are assumed to have the same uniform diameter of $\bar{d}$. We can logically conjecture that all the inserted beams are
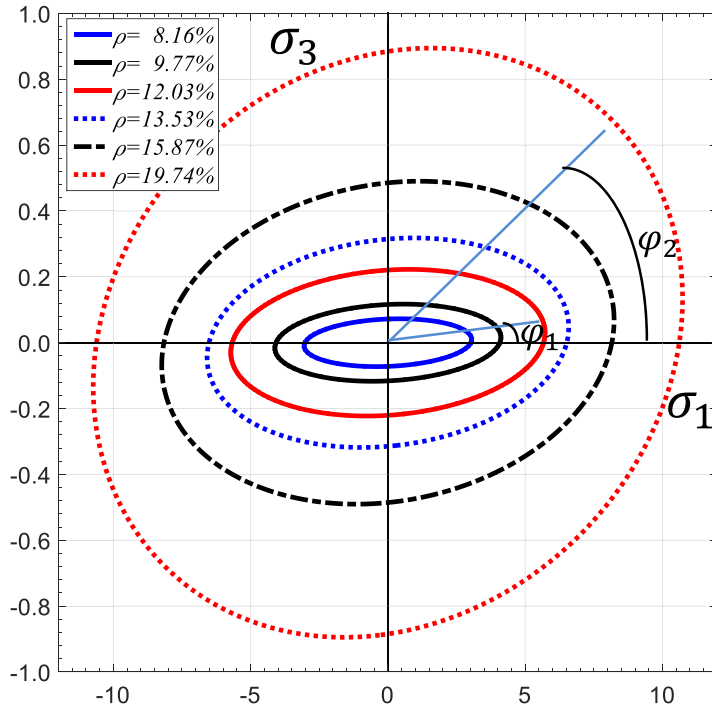
Fig. 14. Yield surface in the plane of anisotropy for stochastic fibre network materials with different relative density.
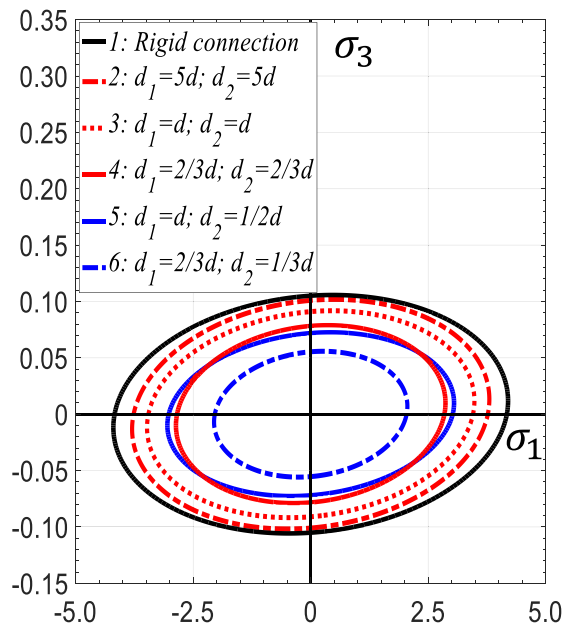

Fig. 15. Yield surface in the plane of anisotropy for stochastic fibre network materials with different treatments of the cross-linkers.

unlikely to yield when the fibre network materials are stretched either in the x or the z direction. The size reduction of the yield surface is because this case allows larger difference between the displacements of the two end nodes of the inserted beams than the previous case (i.e. case 2), and thus more significantly reduces the stiffness and yield strength of the fibre network materials. In the fourth case, all the inserted beams are assumed to have the same diameter of $\frac{2}{3}\bar{d}$ and the fifth treatment assumes that $d_1 = \bar{d}$ and $d_2 = \frac{1}{2}\bar{d}$. As can be seen, overlap occurs on the yield surface between these two cases and the two different treatments do not make a significant difference in the yield surface. In the sixth case, the diameters of

the inserted beams are assumed to be $d_1 = \frac{2}{3}\bar{d}$ and $d_2 = \frac{1}{3}\bar{d}$, and the consequent yield surface is the smallest. In this case, the yielding may be mainly dominated by the plastic deformation of the middle part of the inserted beams.

Fig. 15 demonstrates that the treatment of rigid connection for the cross-linkers can result in significantly overestimated yield strengths in both the x and z directions, and that the treatment for cross-linkers plays a significant role in the mechanical behaviour of fibre network materials. By comparing case six with case five, we can conclude that the treatment of cross-linkers in case five, i.e. $d_1 = \bar{d}$ and $d_2 = \frac{1}{2}\bar{d}$ (which is the treatment adopted in the simulations of this paper), does not cause significant plastic deformation in the middle part of the inserted beams. Otherwise, if the plastic deformation in the middle part of the inserted beams were the dominant deformation mechanism in case five, the yield strength would follow the scaling law: $(Y_{33})_5/(Y_{33})_6 = (\frac{1}{2}\bar{d})^2/(\frac{1}{3}\bar{d})^2 = 2.25$. Therefore, the adoption of $d_1 = \bar{d}$ and $d_2 = \frac{1}{2}\bar{d}$ for the diameters of the inserted beams (i.e. cross-linkers) in this paper is reasonable.

Natural living materials are usually cellular porous materials. Man-made fibre network materials (Huang et al., 2003; Zhang et al., 2008) are widely used in bioscience and biomedical engineering. They are often used as scaffold to replace damaged bones or teeth. Thus, the yield strength of the fibre-network materials is critical in these applications. Markaki and Clyne (2004) conducted a magneto-mechanical simulation of bone growth using the ferromagnetic fibre materials and the application of a magnetic field. The concept that a porous and permeable implant could be treated as a scaffold for tissue growth has been well established (Hutmacher, 2000). The ferromagnetic fibre network in a magnetic field can be regarded as an *active* scaffold as the magnitude of deformation of the fibre arrays can be included and controlled. The investigation on the fibre-network materials would facilitate identification of conditions for the onset of inelastic behaviour and development of models applied in tissue engineering.

6. Conclusion

In this study, a three-dimensional periodic beam model has been developed to investigate the elasto-plastic properties of stochastic fibre network materials with cross-linkers. Periodic boundary conditions have been applied to the model, and the macroscopic stress and strain of the stochastic fibre network materials have been described over a periodic representative volume element. Additional beam elements are inserted at the fibre intersections to represent the cross-linkers. The density of cross-linkers plays a significant role in both the stiffness and strength of the stochastic fibre network materials. The simulation results indicate that the stochastic fibre network materials are transversely isotropic with the properties in the x direction identical to those in the y direction. Interestingly the stochastic beam-network model developed in this study is pressure independent as the response under tension is the same as that under compression when the deformation is small ($\varepsilon \leq 0.6\%$). Based on the total strain energy density, the scalar measures of characteristic stress and strain are applied to reveal the elasto-plastic behaviour. It must be addressed that the homogenized total strain energy density is dependent on the way in which the normalized stresses and strains are scaled back. The elastic regimes of characteristic stress-strain curves collapse along a single master line irrespective of the loading path. The yield stress or strain is defined as the value at the point on the characteristic stress-strain curve at which the tangent gradient is 50% the initial gradient (i.e. the initial Young's modulus). We have incorporated the shear stress components into the yield criterion and the simulation results indicate that the presence of the shear stress only reduces the size of the yield surface in the plane of anisotropy, but does not change the shape. The yield function can be fully calibrated in terms of the uniaxial tension (or compression) response in the x or z direction, instead of complex multiaxial loading responses. The in-plane stiffness and strength are much larger than those in the out-of-plane direction. By changing the density of cross-linkers (i.e. the relative density of the fibre network material) in the model, the degree of strength anisotropy can be adjusted in terms of the tilt angle of the yield surface in the plane of anisotropy. The relative density of the fibre network materials shows a linear relationship with the density of cross-linkers. Thus, the dependence of the stiffness and strength of the stochastic fibre network materials on relative density is the same as that on the density of cross-linkers. The uniaxial yield strength in the x direction is a quadratic function of the relative density of the stochastic fibre network materials when the relative density is smaller (i.e. $\rho \leq 0.2$) and gradually becomes a linear function when $\rho \geq 0.22$. In contrast, the uniaxial yield strength in the z direction is constantly a cubic function of the relative density. The simulation results show strong agreement with our dimensional analysis and are broadly consistent with the relevant experimental results.

References

Alkhader, M., Vural, M., 2009. An energy-based anisotropic yield criterion for cellular solids and validation by biaxial FE simulations. J. Mech. Phys. Solids 57, 871–890.
Ayyagari, R.S., Vural, M., 2015. Multiaxial yield surface of transversely isotropic foams: Part I—modeling. J. Mech. Phys. Solids 74, 49–67.
Banhart, J., 2001. Manufacture, characterisation and application of cellular metals and metal foams. Prog. Mater. Sci. 46, 559–632.
Chen, C., Lu, T.J., 2000. A phenomenological framework of constitutive modelling for incompressible and compressible elasto-plastic solids. Int. J. Solids Struct. 37, 7769–7786.
Chen, C., Lu, T.J., Fleck, N.A., 1999. Effect of imperfections on the yielding of two-dimensional foams. J. Mech. Phys. Solids 47, 2235–2272.

Clyne, T.W., Markaki, A.E., Tan, J.C., 2005. Mechanical and magnetic properties of metal fibre networks, with and without a polymeric matrix. Compos. Sci. Technol. 65, 2492–2499.

Deshpande, V.S., Fleck, N.A., 2000. Isotropic constitutive models for metallic foams. J. Mech. Phys. Solids 48, 1253–1283.

Gibson, L.J., Ashby, M.F., 1997. Cellular Solids: Structure and Properties. Cambridge university press.

Grishanov, S., Tausif, M., Russell, S.J., 2012. Characterisation of fibre entanglement in nonwoven fabrics based on knot theory. Compos. Sci. Technol. 72, 1331–1337.

Hill, R., 1963. Elastic properties of reinforced solids: some theoretical principles. J. Mech. Phys. Solids 11, 357–372.

Huang, Z.M., Zhang, Y.Z., Kotaki, M., Ramakrishna, S., 2003. A review on polymer nanofibers by electrospinning and their applications in nanocomposites. Compos. Sci. Technol. 63, 2223–2253.

Hutmacher, D.W., 2000. Scaffolds in tissue engineering bone and cartilage. Biomaterials 21, 2529–2543.

Jin, M.Z., Chen, C.Q., Lu, T.J., 2013. The mechanical behavior of porous metal fiber sintered sheets. J. Mech. Phys. Solids 61, 161–174.

Johnson, J.B., 1918. Johnson's Materials of construction. John Wiley & sons, Incorporated.

Markaki, A.E., Clyne, T.W., 2005. Magneto-mechanical actuation of bonded ferromagnetic fibre arrays. Acta Mater. 53, 877–889.

Markaki, A.E., Clyne, T.W., 2004. Magneto-mechanical stimulation of bone growth in a bonded array of ferromagnetic fibres. Biomaterials 25, 4805–4815.

Markaki, A.E., Clyne, T.W., 2003. Mechanics of thin ultra-light stainless steel sandwich sheet material: Part I. Stiffness. Acta Mater. 51, 1341–1350.

Picu, R.C., 2011. Mechanics of random fiber networks—a review. Soft Matter 7, 6768–6785.

Qiao, J., Xi, Z., Tang, H., Wang, J., Zhu, J., 2009. Influence of porosity on quasi-static compressive properties of porous metal media fabricated by stainless steel fibers. Mater. Des. 30, 2737–2740.

Redenbach, C., 2009. Microstructure models for cellular materials. Comput. Mater. Sci. 44, 1397–1407.

Sampson, W.W., 2008. Modelling Stochastic Fibrous Materials with Mathematica. Springer Science & Business Media.

Sastry, A.M., Wang, C.W., Berhan, L., 2001. Deformation and failure in stochastic fibrous networks: scale, dimension and application. Key Eng. Mater. 200, 229.

Sill, T.J., von Recum, H.A., 2008. Electrospinning: applications in drug delivery and tissue engineering. Biomaterials 29, 1989–2006.

Silva, M.J., Gibson, L.J., 1997. The effects of non-periodic microstructure and defects on the compressive strength of two-dimensional cellular solids. Int. J. Mech. Sci. 39, 549–563.

Symons, D.D., Fleck, N.A., 2008. The imperfection sensitivity of isotropic two-dimensional elastic lattices. J. Appl. Mech. 75, 51011.

Tsarouchas, D., Markaki, A.E., 2011. Extraction of fibre network architecture by X-ray tomography and prediction of elastic properties using an affine analytical model. Acta Mater. 59, 6989–7002.

Wang, C.W., Berhan, L., Sastry, A.M., 2000. Structure, mechanics and failure of stochastic fibrous networks: Part1—microscale consideration. ASME J. Eng. Mater. Technol 122, 450–459.

Wang, C.W., Sastry, A.M., 2000. Structure, mechanics and failure of stochastic fibrous networks: Part II—network simulations and application. J. Eng. Mater. Technol. 122, 460–468.

Won, Y., Gao, Y., Panzer, M.A., Xiang, R., Maruyama, S., Kenny, T.W., Cai, W., Goodson, K.E., 2013. Zipping, entanglement, and the elastic modulus of aligned single-walled carbon nanotube films. Proc. Natl. Acad. Sci. 110, 20426–20430.

Xi, Z., Zhu, J., Tang, H., Ao, Q., Zhi, H., Wang, J., Li, C., 2011. Progress of application researches of porous fiber metals. Materials (Basel). 4, 816–824.

Youssef, S., Maire, E., Gaertner, R., 2005. Finite element modelling of the actual structure of cellular materials determined by X-ray tomography. Acta Mater. 53, 719–730.

Zhang, Y., Venugopal, J.R., El-Turki, A., Ramakrishna, S., Su, B., Lim, C.T., 2008. Electrospun biomimetic nanocomposite nanofibers of hydroxyapatite/chitosan for bone tissue engineering. Biomaterials 29, 4314–4322.

Zhao, T.F., Chen, C.Q., 2014. The shear properties and deformation mechanisms of porous metal fiber sintered sheets. Mech. Mater. 70, 33–40.

Zhao, T.F., Chen, C.Q., Deng, Z.C., 2016. Elastoplastic properties of transversely isotropic sintered metal fiber sheets. Mater. Sci. Eng. A 662, 308–319.

Zhao, T.F., Jin, M.Z., Chen, C.Q., 2013. A phenomenological elastoplastic model for porous metal fiber sintered sheets. Mater. Sci. Eng. A 582, 188–193.

Zhu, H.X., Hobdell, J.R., Windle, A.H., 2001. Effects of cell irregularity on the elastic properties of 2D Voronoi honeycombs. J. Mech. Phys. Solids 49, 857–870.

Zhu, H.X., Hobdell, J.R., Windle, A.H., 2000. Effects of cell irregularity on the elastic properties of open-cell foams. Acta Mater. 48, 4893–4900.

Zhu, H.X., Knott, J.F., Mills, N.J., 1997. Analysis of the elastic properties of open-cell foams with tetrakaidecahedral cells. J. Mech. Phys. Solids 45, 319–343.

Zhu, H.X., Yan, L.B., Zhang, R., Qiu, X.M., 2012. Size-dependent and tunable elastic properties of hierarchical honeycombs with regular square and equilateral triangular cells. Acta Mater. 60, 4927–4939.